Liquid Crystals
Publication details, including instructions for authors and subscription information:
http://www.informaworld.com/smpp/title~content=t713926090

Pyroelectric investigations of polarization and charge distributions in sandwich cells containing a ferroelectric liquid crystalline polymer

N. Leister; D. Geschke

Online publication date: 06 August 2010

To cite this Article Leister, N. and Geschke, D.(1998) 'Pyroelectric investigations of polarization and charge distributions in sandwich cells containing a ferroelectric liquid crystalline polymer', Liquid Crystals, 24: 3, 441 — 449
To link to this Article: DOI: 10.1080/026782998207271
URL: http://dx.doi.org/10.1080/026782998207271

LIQUID CRYSTALS, 1998, VOL. 24, NO. 3, 441–449

Pyroelectric investigations of polarization and charge distributions in sandwich cells containing a ferroelectric liquid crystalline polymer

by N. LEISTER* and D. GESCHKE

Universität Leipzig, Fakultät für Physik und Geowissenschaften,
Institut für Experimentelle Physik I, Abteilung Polymerphysik, Linnéstraße 5,
D-04103 Leipzig, Germany

(*Received 16 July 1997; in final form 18 September 1997; accepted 1 October 1997*)

With the laser intensity modulation method (LIMM), polarization and charge profiles in sandwich cells containing the ferroelectric liquid crystal side group polymer LCP1 have been investigated. In a sample with a thickness larger than the helical pitch, contributions to the polarization profile due to surface anchoring were found. Additional contributions inside the cell occurred. The validity of the results, concerning numerical deviations in the deconvolution process of the pyrospectra, has been tested by simulations. The influence of space charges for measurements with a static external electrical field is discussed, giving contributions to the profile in addition to those arising from polarization.

1. Introduction

Ferroelectric liquid crystals (FLCs) have been subject to much interest in recent years. One of the common methods for characterizing an FLC material is the measurement of pyroelectric properties [1]. Hereby the value of the spontaneous polarization can be determined. Heat generated inside the FLC cell by absorption of laser light causes changes of the polarization with temperature and, as a consequence, a pyroelectric current. An integrated value of polarization over the cell thickness is determined, therefore uniform polarization is required, which can be obtained in surface stabilized cells or by orientation of molecules under an external electric field.

As an expansion of this technique the laser intensity modulation method (LIMM) [2, 3] allows pyroelectric investigations of polarization and charge profiles over the cell thickness. In this case the absorption of intensity-modulated light takes place at the surface of the cell only, and the penetration depth of the thermal waves is varied by changing the modulation frequency. Therefore a thermal scan over sample thickness can be realized.

The resulting state of the FLC in a cell is obtained by a minimum of the free energy, which has contributions from elastic energy, surface energy terms and field effects. In cells with a thickness larger than the helical pitch and for weak external fields, a non-uniform orientation over the cell thickness is expected, dependent on material parameters and surface properties. These effects can be investigated by the LIMM technique.

The first LIMM investigations on liquid crystalline polymers were carried out on a nematic material with a frozen-in polarization distribution obtained by thermal poling [4]. Our measurements applying this technique to the ferroelectric liquid crystalline polymer (FLCP) P8*S have been reported elsewhere [5]. In the following text results for a different FLCP with better resolution are presented. Furthermore differences in the behaviour of the materials are discussed and some results similar to those obtained previously can be given in more detail.

2. Experimental

2.1. *Method*

The laser intensity modulation method, LIMM, has been developed by Lang and Das-Gupta [2]. Details of the experimental set-up and the numerical deconvolution of the spectra used here have been described elsewhere [4–7].

The principle of the method is as follows. A sample with a thin metal layer on its surface is irradiated by an intensity-modulated laser beam; the metal layer acts simultaneously as a light absorber and an electrode. A heat wave is generated by light absorption and penetrates into the sample, the penetration depth depending on the modulation frequency. For small frequencies the whole sample is heated almost homogeneously; for high frequencies the heated range is concentrated near the irradiated side. Variation of the modulation frequency

*Author for correspondence.

allows a thermal scan of the sample. Charges and dipoles inside the sample react to heating, causing a measurable pyroelectric current on the electrodes.

In the experimental set-up the beam of a helium/neon laser ($\lambda = 633$ nm) with a nominal output of 25 mW, is intensity-modulated sinusoidally by an acousto-optic modulator (AOM). The laser beam is incident on the upper metal layer, while the rear side of the sample is thermally contacted to a heat sink. The pyroelectric current is detected and converted to a voltage by a current to voltage converter (CVC) with amplification factor 1 MV A^{-1}. This voltage is detected by a lock-in amplifier with respect to the phase of the incident light. The AOM is driven by a function generator which also produces the reference frequency for the lock-in amplifier; the function generator and lock-in amplifier are controlled by a computer. An external electric field can be applied by a battery driven voltage source which is coupled to the CVC through a capacitor.

A quantitative description is given by the following equations. The pyroelectric current I_p for a fixed modulation frequency ω is [6]:

$$I_p(\omega) = \frac{A}{L} \int_0^L r(z) \frac{\partial T(\omega, z)}{\partial t} \mathrm{d}z, \qquad r(z) = g(z) + (\alpha_\varepsilon - \alpha_z)\varepsilon\varepsilon_0 E(z) \tag{1}$$

with A as electrode area, L as sample thickness, and $T(\omega, z)$ as temperature profile at modulation frequency ω (see below); $r(z)$ is the distribution searched for and has contributions from the pyroelectric coefficient $g(z) = \mathrm{d}P_s/\mathrm{d}T$ and from the electric field $E(z)$ caused by charges in the sample. $\alpha_\varepsilon = 1/\varepsilon\, \partial\varepsilon/\partial T$ is the temperature coefficient of permittivity and $\alpha_z = 1/z\, \partial z/\partial T$ is the temperature coefficient of thickness.

The field $E(z)$ is given as:

$$E(z) = R(z) - \bar{R}, \qquad R(z) = \int_0^z \rho_{ges}(\zeta)\, \mathrm{d}\zeta, \qquad \bar{R} = \frac{1}{L} \int_0^L R(z)\, \mathrm{d}z, \quad \rho_{ges}(z) = \rho(z) - \frac{\mathrm{d}P_r}{\mathrm{d}z} \tag{2}$$

where $\rho(z)$ is the charge density. If the polarization is locally compensated by charges [$\rho(z) = \mathrm{d}P_r/\mathrm{d}z$], then $E(z) = 0$ holds and, therefore, $r(z)$ has contributions only from the pyrocoefficient $g(z)$. In general the contributions from space charges and dipole polarization to the pyrosignal are not distinguishable from the measured data alone [3]; further knowledge is needed. For example a pyrosignal which occurs in the temperature range of the SmC* phase and changes drastically at the phase transition point can be attributed to polarization.

The temperature profile $T(\omega, z)$ is given by a solution of the one-dimensional heat conduction equation [6] (here $z = 0$ is the front side and $z = L$ is the rear side of the sample).

$$T(\omega, z) = \frac{q - \eta_a}{\kappa K} \frac{\cosh[K(L - z)] + a_L \sinh[K(L - z)]}{(a_0 + a_L)\cosh(KL) + (1 + a_0 a_L)\sinh(KL)} \tag{3}$$

where

$$a_{0,L} = \frac{H_{0,L}}{\kappa K}, \qquad K = (1 + \mathrm{j})\left(\frac{\omega}{2\chi}\right)^{1/2}, \qquad \chi = \frac{\kappa}{\rho c_p}.$$

Here K is the wave number of the thermal waves, q – the incident heat flux, η_s the absorbtivity of the metal layer, κ the thermal conductivity, ρ the volume density, c_p the specific heat and χ the thermal diffusivity.

H_0 and H_L are the heat transfer coefficients at the front side and the rear side of the sample, respectively. The magnitude of these coefficients depends on the interaction of the cell with its environment. In the thermally isolated case $H_0 = 0$ and $H_L = 0$. (In real situations H_0 and H_L are small, but not zero because of thermal radiation to the surrounding air.) Where permanent heat generation on the sample surface takes place, static heating of the sample occurs. The sample temperature may be several K above the environmental temperature. In the case of FLC materials $r(z)$ generally depends on temperature. This may lead to significant errors in measurement, especially near phase transition points, where large changes of $r(z)$ with temperature may take place.

For the thermally contacted case, the rear side of the sample is mounted on a heat sink. Therefore $H_0 = 0$ and $H_L = \infty$. (In real situations H_0 is small, about 5 J s^{-1} m^{-1} K^{-2}, and H_L is large, but finite, in the range of 10^3–10^4 J s^{-1} m^{-1} K^{-2}.) In this case the static heating of the sample is small and the sample temperature differs only slightly from ambient. Therefore the thermally contacted case is preferred in investigations of FLC.

From the measured spectrum of the pyroelectric current I_p, the distribution $r(z)$ can be obtained by numerical deconvolution techniques. The Tikhonov regularization method is used here [7]. Knowledge of the temperature profile $T(\omega, z)$ is needed to obtain $r(z)$ from I_p [see equation (1)]. $T(\omega, z)$ depends on material parameters [see equation (3)], the thermal conductivity κ and the thermal diffusivity χ as well as on the heat transfer coefficient H_L, which can be determined in an iterative procedure by minimizing the residues of the deconvolution results as described by Steffen *et al.* [7].

The experimental set-up for normal pyroelectric measurements on FLC (see, e.g. [8, 9]) is very similar to the LIMM set-up [5, 6], despite the fact that a fixed modulation frequency is used there. On the other hand it should be emphasized that LIMM compared with

usual investigations involves additional factors, such as time consuming measurements, deconvolution of spectra and special requirements on the cell type.

2.2. *Samples*

A number of requirements on the cell must be fulfilled. Equation (3) for the temperature profile $T(\omega, z)$ is valid only if heat generation takes place in a very thin layer at $z = 0$. Additional locations of light absorption which are different from the metal electrode (e.g. inside the LCP layer or in a sheet of cover glass) would destroy this relation between the penetration depth of the thermal waves and the modulation frequency of the light, which is necessary for a thermal scan of the sample. Therefore the electrodes must be completely non-transparent and should be located on the outer surface of the sample. A set-up with semi-transparent electrodes as described in [8] for normal pyroelectric measurements, with the advantage of allowing electro-optical investigations on the same samples, would not be suitable for LIMM.

The pyroelectric current is detected by a current to voltage converter (CVC). At high modulation frequencies the capacitive impedance of the sample becomes comparable in size to the input impedance of the CVC. Therefore the amplification factor of the CVC is influenced by the sample capacity. The electrode area has to be minimized in order to achieve a low sample capacity.

Static heating of the sample has to be avoided. As discussed above, the thermally contacted case with the sample mounted on a heat sink has to be realized. A cell type possessing a relatively thick cover glass on the rear side would hinder good thermal contact to the heat sink and is therefore not suitable.

Due to these reasons, a commercially available ITO cell largely used in investigations on LC materials cannot be used. Gold coated glass plates also seem to be an impractical choice. This leads to the disadvantage that comparison with the results of other measurement techniques is rather difficult. For example, optical microscopy can only be performed on the parts of the samples which are outside the electrode area.

The type of cell used here (see figure 1) is an improved version of the one described by Steffen *et al.* [4]. The FLC layer is placed between thin polymer foils, which are vacuum deposited with metal electrodes on the outside. These electrodes have a central area of circular shape with a diameter of 2 mm according to the size of the laser beam and a cross of 4 narrow lines for electrical contact. The LCP is brought between the foils and heated into the isotropic phase. The sample is carefully pressed together until the desired thickness is reached; then the sample is slowly cooled down. For the rather thin sample (12 μm LCP layer in contrast to 25 μm in former investigations [4]) no spacer is used. Because of the high viscosity of polymeric LC materials, the sample is mechanically stable without a spacer ring. The area of the LCP layer is distinctly larger (diameter 8 mm) than the electrode area, so that thickness variations at its border do not influence the measurement.

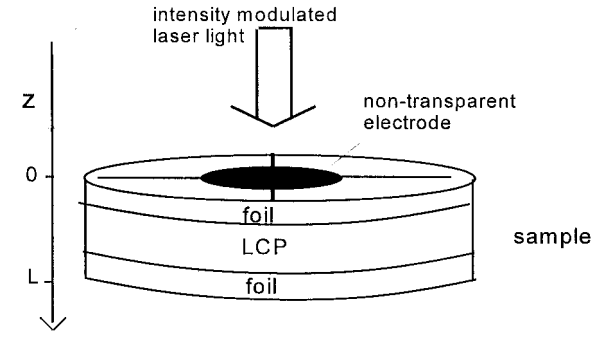

Figure 1. Schematic illustration of the cell structure.

Instead of gold alone [4], the electrodes now include an additional bismuth layer. Bismuth has high absorptivity η_a [10]. The same incoming laser intensity then results in a larger amount of heat generation and therefore an increased signal magnitude. For foil material 2·5 μm Mylar® was used throughout instead of the 7·5 μm Kapton® foil, which was used in former investigations on a nematic LCP [4] and for most samples of ferroelectric P8*S [5]. This was done in order to increase sensitivity. The LCP layer (the region of the sample being of interest) is nearer to the surface and therefore reached even at high modulation frequencies and correspondingly low penetration depths. Therefore a larger part of the spectrum contains contributions from the LCP layer, compared with cells where Kapton® foil was used, thus increasing spatial resolution. In addition, the same amount of heat generated at the surface is spread over a smaller volume in order to reach the same position inside the LCP layer and therefore the signal amplitude is increased.

Effects observed for LCP1 are smaller by about a factor of 8 compared with P8*S [5] under the same conditions. This can be attributed to a smaller pyroelectric coefficient. Therefore the combination of bismuth electrodes and Mylar® foil is necessary to get a sufficient signal to noise ratio. Common LC cells have thin polymer layers between the electrode and the LC. The cell type used here, in respect of its principle structure, is similar to a standard cell. On the other hand, the special requirements of the LIMM method are taken into consideration.

The LCP material was purchased from Merck Ltd, Poole, trade name LCP1. It is characterized by a glass transition temperature −7·2°C, the SmC* to isotropic phase transition at 76·8°C and a chain length of about

40 units (Merck Ltd data sheet). The chemical structure is shown in figure 2. The LCP is put into a cell in the isotropic phase and slowly cooled. Polarization microscopy shows a fine grained anisotropic texture. Repeated heating and cooling cycles near the phase transition point (without applied field) for about one day produce a change in the texture. A stripe shaped texture results but no monodomain can be obtained. In order to exclude influences arising from peculiarities of the individual sample, three samples with nearly the same properties were investigated; similar results were obtained for all three. Typical data are presented here.

3. Results and discussion

3.1. *Surface effects*

Figure 3 shows a measured pyroelectric spectrum of a sample without external field. It consists of a real and an imaginary part because the amplitude as well as the phase of the signal with respect to the modulated light were recorded. Compared with measurements on the ferroelectric polysiloxane P8*S [5] for the same cell set-up (use of Mylar foil) the spectrum has a similar but not identical shape with the real part maximum at about 4 kHz. Furthermore the spectrum differs in magnitude by about a factor of 8 and in sign. For cells using Kapton® foil, comparison of results of measurements on both materials leads to the same results, while signal magnitude and position of maximum differ with respect to Mylar® cells as discussed in the previous section.

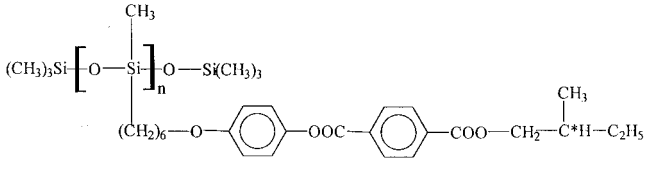

LCP 1 g -7.2 °C SmC* 76.8 °C I

Figure 2. The chemical structure of the polymer with the trade name LCP1, $n \approx 40$.

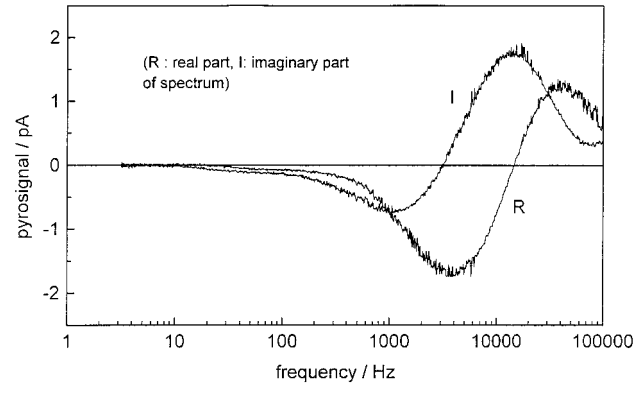

Figure 3. Measured spectrum of the pyroelectric current; measurement at 25°C without external field. Sandwich cell: 12 μm LCP layer and two 2·5-μm-thick Mylar® foils.

Only one component of the polarization vector has an effect on the signal. This vector is defined as $\mathbf{P} = P[\mathbf{n} \times \mathbf{x}]$, where $\mathbf{n}$ is the director and $\mathbf{x}$ the normal to the smectic layers. The different sign of the pyrospectra obtained from both materials can be attributed to a different orientation of the polarization vector. Change in magnitude may also be due to different orientation, if $\mathbf{P}$ is not perpendicular to the cell surface. Therefore no absolute values are given.

The numerical evaluation of the distribution using Tikhonov regularization leads to a result for each, real and imaginary, part of the measured spectrum. Agreement of both distributions confirms the result. The resolution of the method is high near the irradiated side and decreases with rising penetration depth of the thermal waves. Evaluation of the distributions often leads to deviations on the rear side caused by numerical artefacts. It is therefore necessary to turn the sample around and irradiate it from the other side. Distributions evaluated from both experiments should give similar results in the middle part of the sample. This agreement is a further confirmation of the results.

The iterative procedure for determining the thermal parameters (see above) in the case of the sample presented here leads to a thermal diffusivity $\chi = 85 \times 10^{-9}\ \mathrm{m^2\ s^{-1}}$ and a thermal conductivity $\kappa = 0{\cdot}15\ \mathrm{J\ s^{-1}\ m^{-1}\ K^{-1}}$. In order to realize the thermally contacted case, in former investigations the sample was stuck onto a heat sink using a silver dispersion. As this sticking procedure often led to damage to the electrodes, it was omitted here. Therefore, less intimate contact with the heat sink and a smaller heat transfer coefficient are expected. The values for H_L taken from the iteration are in agreement with these expectations. In the case of the sample for which results are presented here, these values are $1{\cdot}0 \times 10^3\ \mathrm{J\ s^{-1}\ m^{-1}\ K^{-2}}$ (for all measurements by irradiation from one side) and $7{\cdot}0 \times 10^3\ \mathrm{J\ s^{-1}\ m^{-1}\ K^{-2}}$ (for all measurements by irradiation from the other side), compared with former values of typically 1·0 to $1{\cdot}5 \times 10^4\ \mathrm{J\ s^{-1}\ m^{-1}\ K^{-2}}$. In the case of the smaller value ($1{\cdot}0 \times 10^3\ \mathrm{J\ s^{-1}\ m^{-1}\ K^{-2}}$) a static heating of about 1·5 K may result. As measurements are performed in a temperature range where no drastic changes of $r(z)$ with temperature are expected, there should be no significant errors.

The sample thickness is 17 μm, consisting of two Mylar® foils (each one 2·5 μm) and a 12 μm LCP layer. The thickness of the evaporated metal layers is about 100 nm.

Figure 4 shows a distribution consisting of the deconvolution results from two measurements. The sample was irradiated from each side and the results taken from

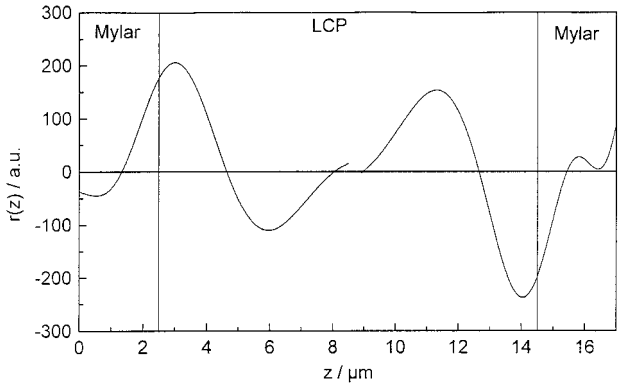

Figure 4. Distribution $r(z)$: results of the deconvolution of the spectrum in figure 3 (right part) and of a measurement with laser irradiation of the other surface [left part; corresponding spectrum shown in figure 6(*a*)].

the irradiated side to the middle of the sample. The right part corresponds to the spectrum shown in figure 3. Two maxima can be seen at the boundary between the LCP layer and the polymer foil which were also found for measurements on P8*S [5], and in addition to these, two further maxima somewhat smaller and of opposite sign inside the cell, which do not exist or at least are much smaller than the boundary parts in the case of the material P8*S.

The SmC* phase is characterized by a layer structure with a tilt of the molecules to the layer normal. A single layer has a resulting spontaneous polarization [11], which is perpendicular to the layer normal and to the plane given by the tilt and the layer normal. In the bulk, the polarization vectors of the layers lie on a helix. Typical layer thickness is in the order of a few nanometres and a typical pitch of the helix a few micrometres. The lateral resolution of the measurement is given by the electrode area (diameter 2 mm). Therefore for planar geometry, with the layers perpendicular to the cell surface, a mean value of zero polarization would be seen in the case of the helical structure.

At the boundary between the LCP layer and the foil, because of surface anchoring, the helix is unwound and a non-zero polarization is expected. For parallel orientation of the mesogenic side groups on the surface and the smectic layers perpendicular to the surface, the polarization vector also points in this direction. The tilt of the molecules with respect to the surface means that the polarization is not perpendicular to the surface, and the relevant component of this vector has a smaller value leading to a smaller signal. Therefore, besides a smaller pyrocoefficient, a different orientation of the molecules may also contribute to the differences in signal magnitude observed for LCP1 compared with P8*S [5].

In cells with a thickness larger than the helical pitch, a range of zero polarization in the inner parts of the layer is expected. The signal at both boundaries may be of the same sign (parallel anchoring; at one surface the polarization points inward and at the other one outward) or of different sign (symmetrical anchoring). The disclination lines may also have an influence on the signal as dislocations in ferroelectrics contain polarization charges. In the experimental result the signal parts at the boundary can be interpreted as polarization because of symmetrical surface anchoring.

The fact that the boundary maxima reach into the Mylar® foil may be due to the numerical deviations caused by the deconvolution procedure. Equation (1) is a Fredholm integral equation of the first kind. The deconvolution is a so called 'ill-posed problem' [2]. A number of different solutions exist all of which satisfy the input data within experimental accuracy, among them such ones having strong oscillations. In order to avoid such oscillations and to find a good solution, smooth distributions are preferred in the deconvolution procedure. This leads to acceptable approximations, but on the other hand systematic deviations in the results take place. For example, steep slopes appearing in the real distribution are smoothed out and widened. The behaviour of the deconvolution results for the Tikhonov regularization technique have been extensively investigated by Steffen *et al.* using simulated data [7, 12].

Here results of a simulation are given, using parameters typical for the LCP cell, in order to illustrate the validity of the experimental result given above. A distribution given by an analytical expression is used. For this distribution the pyroelectric spectrum is calculated using equation (1). White noise may be added to this spectrum. The Tikhonov regularization is applied to the spectrum and the deconvolution result can be compared with the original distribution.

A cell thickness of 15 μm was chosen for the simulation, with an assumed LCP layer of 10 μm. A distribution with two contributions of opposite sign each 2·5 μm away from the surfaces was chosen. Parts of cosinus curves with a constant factor added have been used, having a step at the boundary and a smooth decrease to the inner side. This should be similar to the experimental behaviour where a step between non-polar polymer foil, with a maximum of the polarization at the boundary between foil and LCP layer, is expected, and a gradual decrease of polarization with rising distance from the boundary.

The result of the simulation is shown in figure 5. For the signal part near the irradiated side, the step from 0 to 1 on the right side is smoothed and widened, and the magnitude of the maximum differs, but the smooth decrease on the left side is reproduced almost correctly. In contrast to this, the signal part near the rear side is strongly widened because of resolution decrease of the

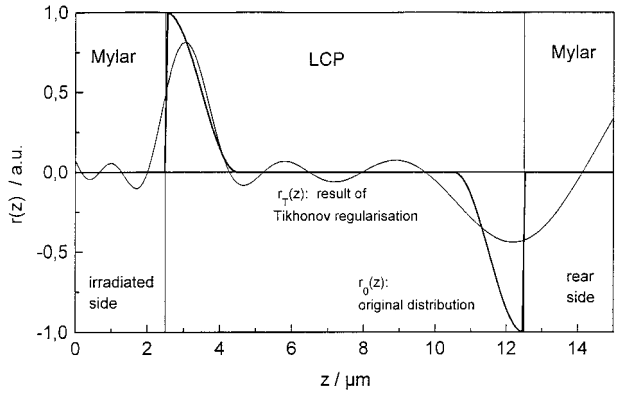

Figure 5. Result of a simulation: original distribution $r_0(z)$ given by an analytical expression (thick line). Distribution $r_T(z)$ (thin line) was obtained by calculating a spectrum $I_p(\omega)$ from $r_0(z)$ and making use of Tikhonov regularization to get a distribution again.

method with rising penetration depth. Inside the cell, where the original distribution was set to zero, small oscillations can be seen, but of much smaller magnitude compared with the signal at the boundaries.

The result given above was obtained without adding noise to the simulated spectrum. Noise amplitudes in the range of 1–3% lead to a slightly larger broadening of the peaks and to a slight rise in magnitude of the oscillations inside the sample. The noise of the measured spectra was determined to be about 2%.

The result of the simulation leads to the following conclusions concerning the experimental data. The fact that the signals at the boundary between LCP and Mylar® reach into the Mylar® foil is caused by numerical widening of a step in the distribution. The small oscillations at the cell surface are also caused by numerical effects. The width of the polarized region near the boundary is slightly widened by numerical effects. The possibility that the inner parts of the distribution are numerical artefacts cannot in principle be excluded. On the other hand, the size of these contributions makes this improbable and they should be based on real effects in the sample. Nevertheless an explanation of these inner maxima located about 3·5 µm away from the surface of the LCP layer is difficult. They may be caused by the disclination lines, but those should be located closer to the surface.

In the texture that was observed by polarization microscopy, no monodomain was obtained. In the case where there exist states with different orientations of the molecules at the surface, but of equal energy, a multi-domain structure with a part of the domains in each state would lead to a mean polarization value of zero over a large area. The fact that a non-zero polarization is measured here seems to point out that a certain orientation is preferred, and the contributions of the single domains add up to the resulting signal.

3.2. *Field effects*

The same sample was exposed to an external electric field. Figure 6 (*a*) shows the real part of the pyrospectra for measurements without field and with voltages of both signs. While the degree of change in the spectra is not quite obvious at first sight, the behaviour of the sample can be better understood if the difference between the spectra with and without field is calculated. Figure 6 (*b*) shows the difference between the + 54 V and the 0 V spectrum, as well as the difference between the − 54 V and the 0 V spectrum. These two curves are of opposite sign, but quite similar shape, having a maximum in the high frequency range > 10 kHz. Therefore the spectra in figure 6 (*a*) can be interpreted as composed of two contributions: the zero voltage signal is still present and overlaps with the additional contribution shown in figure 6 (*b*). The high frequency range corresponds to a low penetration depth, where the thermal waves do not reach the LCP layer, but remain inside the Mylar® foil.

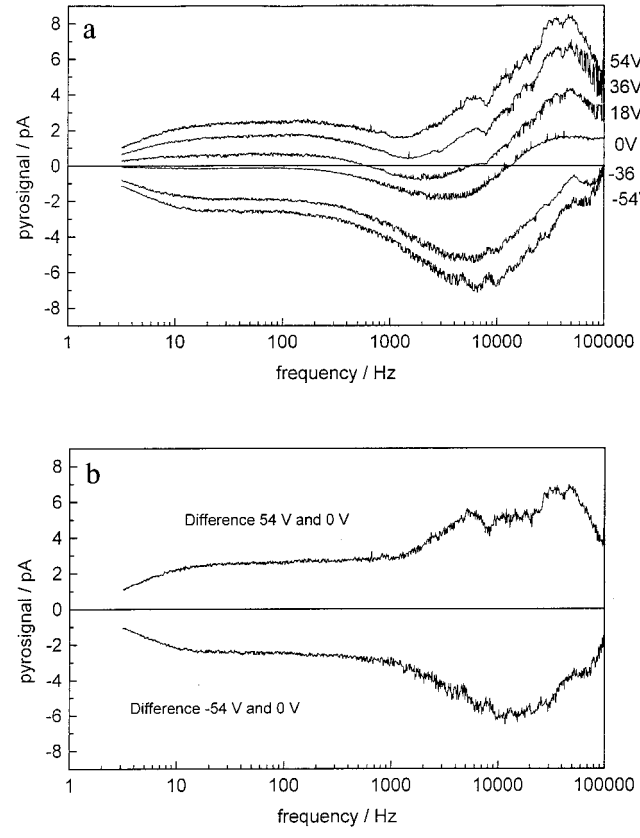

Figure 6. (*a*) Real parts of pyroelectric current spectra for measurements without field and with voltages ranging from − 54 to + 54 V. (*b*) Difference of spectra at 54 and 0 V, and at − 54 and 0 V.

The deconvolution procedure, using the same set of parameters as for the measurements without field, leads to sufficiently small residues. Figure 7 shows the part of the resulting distributions inside the Mylar® foil and inside the LCP layer near the boundary. While the signal size at the boundary between the LCP and the foil changes only by a small amount, there are additional contributions inside the Mylar® foil, with different sign corresponding to the sign of the voltage. These results confirm the assumption that the distribution can be seen as composed of two overlapping parts, one inside the foil and the other one at the boundary.

As Mylar® itself is not a pyroelectric material, the corresponding contributions to the signal should not be caused by the pyrocoefficient $g(z)$, but by the internal field $E(z)$ due to an inhomogeneous charge distribution $\rho(z)$ in the sample. These charge layers can be attributed to screening effects (see, e.g. [13]). Charges due to impurities inside the sample move to the boundaries influenced by the external field. On the other hand, it cannot be excluded that charges also arise from impurities inside the polymer foil or that charges from the electrodes drift into the polymer foil. In the case of a pyrosignal caused by charges alone and having no contributions from dipole polarization, the pyrocoefficient $g(z)$ would have zero value and the distribution $r(z)$ would be directly proportional to the field $E(z)$ [see equation (1)]. In this case the charge distribution $\rho(z)$ can be obtained by differentiation of $r(z)$.

As the material Mylar® is not pyroelectric, $g(z)=0$ holds at least for values of $z<2{\cdot}5$ μm. Furthermore, the distributions shown in figure 7 comprise only minor changes at the boundary between foil and LCP layer. The field is assumed to be too weak to overcome the anchoring. Therefore difference spectra with and without field may be calculated, and from the resulting spectrum a distribution can be obtained by usual deconvolution and the distribution can be differentiated. For small values of z, the result can be interpreted as charge distribution, while inside the LCP layer distortion of the helix will give contributions to $r(z)$ and there the interpretation as charge distribution is not valid. Figure 8 shows a result obtained in this way. The difference of the spectra at -54 V and at 0 V, shown in figure 6(*b*), has been used. The first curve given in figure 8 is the distribution $r_{\mathrm{diff}}(z)$ obtained from this spectrum. The second curve is the charge distribution $\rho(z)$ obtained by differentiation of $r_{\mathrm{diff}}(z)$. $\rho(z)$ has a maximum in negative sign at the boundary between foil and LCP and a maximum in positive sign at the outer surface.

It should be remembered that the numerical deviations discussed above have even larger influence on the differentiated distribution. If a smoothed and widened distribution is differentiated, the result is not expected to be very accurate. Therefore it is assumed that the $\rho(z)$ presented here is strongly broadened and 'washed out'. In reality the charge layers should be much narrower and located on or near both surfaces of the Mylar® foil. An alternative way to determine $\rho(z)$ would be to use a different formula instead of equation (1), relating I_{p} directly to $\rho(z)$ in the case of $g(z)=0$ and $P(z)=0$. It is then possible to obtain $\rho(z)$ directly from the deconvolution of the spectra [12]. Future investigations will test whether this leads to better results.

The saturation fields for helix unwinding in ferroelectric LCP materials are typically in the range 10–15 V $\mu\mathrm{m}^{-1}$ [14]. But even at smaller field strengths the helix will be distorted by the field resulting in a non-zero effective polarization. In the present case, in the absence of charges, a field inside the LCP layer of $E=2{\cdot}5$ V $\mu\mathrm{m}^{-1}$ would result for $V=54$ Volt (with $\varepsilon=3{\cdot}25$ for Mylar® and $\varepsilon=6$ for the LCP material).

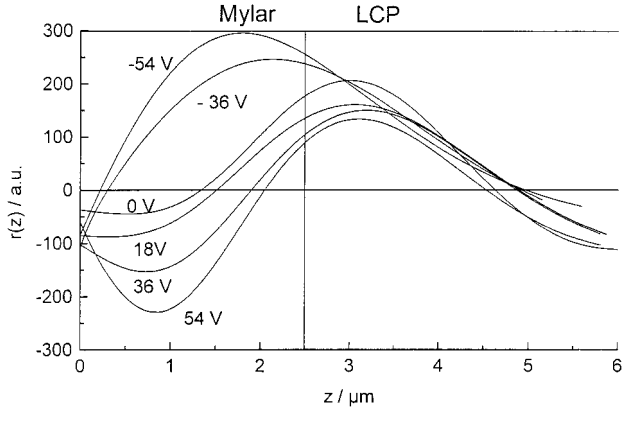

Figure 7. Results of the deconvolution of the spectra in figure 6(*a*) (shown in the region near the irradiated surface only).

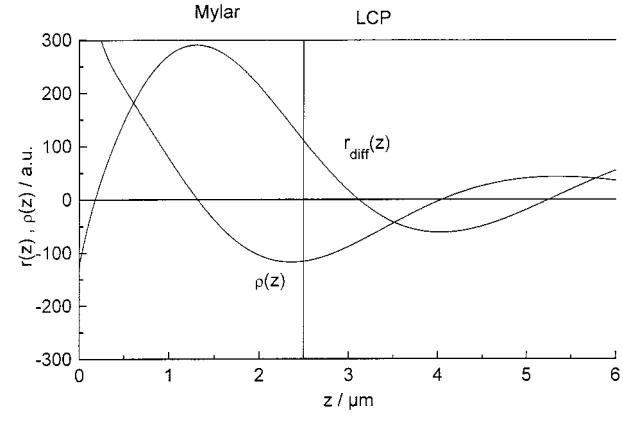

Figure 8. Distribution $r_{\mathrm{diff}}(z)$ obtained from the deconvolution of the difference of the spectra at -54 V and at 0 V shown in figure 6(*b*). Charge distribution $\rho(z)$ was obtained from differentiation of $r_{\mathrm{diff}}(z)$. Both curves are shown in the region near the irradiated surface only.

Because of the screening caused by the charge layers, the actual field is assumed to be somewhat smaller. Exact knowledge of $\rho(z)$ would allow the calculation of this field. In the present case no absolute values of $\rho(z)$ can be given, as this requires knowledge of α_ε and α_z [see equation (1)], which have not been determined for this material. Besides, the field is big enough, so that a change in the inner part of the distribution takes place. Figure 9 shows a complete distribution for applied voltage (−54 V), composed of measurements from both sides. A shift in relative magnitude of the inner maxima can be seen. The signal is shifted in the same direction as for the contributions inside the Mylar®. An influence of the screening charges would lead to an opposite effect here. An interpretation of the exact signal shape is difficult due to the unknown origin of the inner maxima. If these inner maxima are caused by disclination lines, these lines may change under the influence of the field.

For further investigations the question arises, what spatial resolution may be reached by the method? Lang [3] has made simulations using δ-distributions, calculating the spectrum and from this the distribution again. The broadening of the results was taken as a measure for the resolution. Steffen *et al.* [7, 13] used distributions of non-zero width for simulations. They determined a theoretical limit for the spatial resolution according to the equation:

$$\mathrm{NLW_{th}} = c\ \eta_{\max}\ \sigma_{\mathrm{th}}^{1/2} \qquad (4)$$

where $\mathrm{NLW_{th}}$ is the natural linewidth. Distributions having a half width smaller than the $\mathrm{NLW_{th}}$ cannot be distinguished by the method. $\eta_{\max}$ is the distance of the distribution maximum from the irradiated surface, σ_{th} is the noise amplitude of the spectrum and c is a constant, which was determined to be 0·255. Equation (4) is not valid directly at the surface of the sample, where the resolution is limited by the maximum modulation frequency, which corresponds to a minimum penetration depth. In the present case, for $f_{\max} = 100$ kHz the surface resolution is about 0·2 μm. For the sample investigated here, the $\mathrm{NLW_{th}}$ can be calculated, using equation (4) and a noise value of 2%, resulting in $\mathrm{NLW_{th}} = 0{\cdot}1$ μm at the interface between LCP layer and Mylar® foil and $\mathrm{NLW_{th}} = 0{\cdot}3$ μm in the middle of the LCP layer. This may be improved by further reduction of the foil thickness (but this will make the construction of mechanically stable cells even more difficult) and further noise reduction. On the other hand the experimental results concerning the resolution are still above the theoretical limit, which can be attributed to the restriction to smooth distributions in the deconvolution procedure. Ways of improvement have to be worked out.

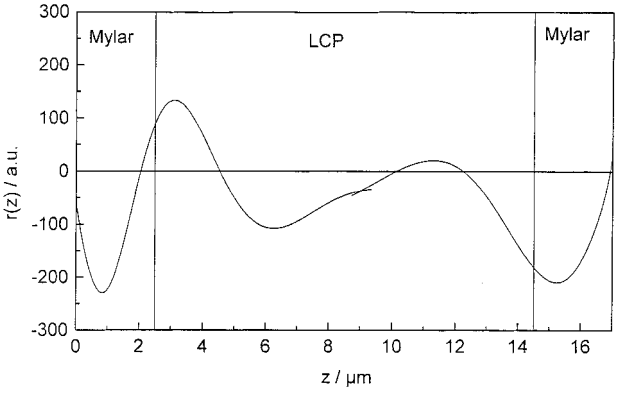

Figure 9. Distribution $r(z)$ at −54 V, shown over the whole sample thickness. Composed of deconvolution results from two measurements; left part the same as in figure 6 (*a*).

Future experimental investigations will comprise further variation of the foil thickness, which is expected to have an influence not only on the spatial resolution but also on the charge effects. The thickness of the LCP layer will also be varied. While the surface contributions should remain the same, the effects inside the LCP layer may change and therefore may help to clarify whether there are numerical artefacts or real effects. Measurements on P8*S at different temperatures did lead to changes of the spectrum [5]. The question as to whether similar effects can be seen for LCP1 is also of interest and may help further to understand these effects. More different materials will be investigated to look for individual differences.

4. Conclusions

With LIMM, spatially resolved charge and polarization profiles for a ferroelectric liquid crystalline polymer in a sandwich cell using Mylar® foil have been measured. For measurements without external field, the surface interaction of the molecules has been investigated. Symmetrical surface anchoring was found as in former investigations on the material P8*S, although the magnitude and sign of the pyrosignals differ. Additional contributions to the distribution inside the LCP layer occur for LCP1 but are difficult to explain.

The validity of the results, concerning numerical deviations in the deconvolution process of the pyrospectra, has been tested by simulations. From these simulations the distribution is assumed to be slightly smoothed and widened, but in qualitative agreement with the real situation.

For measurements with a static applied electrical field, contributions of charges due to screening effects were found as for P8*S. A charge distribution $\rho(z)$ was calculated, using the difference in pyrospectra with and without field, obtaining a distribution $r_{\mathrm{diff}}(z)$ from this and differentiating the distribution. $\rho(z)$ can be interpreted as having charge layers near the inner and outer

surface of the Mylar® foil. The contributions from surface anchoring to the distribution $r(z)$ remain the same under applied field, while inside the LCP layer small changes can be seen despite the screening of part of the field by the charges.

Further investigations with systematic variation of cell parameters and materials should allow a deeper insight.

Financial support by the Deutsche Forschungsgemeinschaft within the research project No. Ge 718/4-1 is gratefully acknowledged.

References

[1] Yu, L. H., Lee, H., Bak, C. S., and Labes, M. M., 1976, *Phys. Rev. Lett.*, **36,** 388.
[2] Lang, S. B., and Das-Gupta, D. K., 1986, *J. Appl. Phys.*, **59,** 2151.
[3] Lang, S. B., 1991, *Ferroelectrics*, **118,** 343.
[4] Steffen, M., Bloß, P., Schäfer, H., Winkler, M., and Geschke, D., 1995, *Liq. Cryst.*, **19,** 93.
[5] Leister, N., Geschke, D., and Kozlovsky, M. V., *Mol. Cryst. liq. Cryst.* (in press).
[6] Bloß, P., and Schäfer, H., 1994, *Rev. sci. Instr.*, **65,** 1541.
[7] Steffen, M., Bloß, P., and Schäfer, H., 1994, in Proceedings of the 8th International Symposium on Electrets, edited by J. Lewiner, D. Morisseau and C. Alquié, p. 200.
[8] Kocot, A., Wrzalik, R., Vij, J. K., and Zentel, R., 1994, *J. appl. Phys.*, **75,** 728.
[9] Helgee, B., Hjertberg, T., Skarp, K., Andersson, G., and Gouda, F., 1995, *Liq. Cryst.*, **18,** 871.
[10] Bauer, S., Ploss, B., 1990, *J. appl. Phys.*, **68,** 6361.
[11] Meyer, R. B., Liébert, L., Strzelecki, L., and Keller, P., 1975, *J. Phys. (Paris)*, **36,** L-69.
[12] Steffen, M., 1996, PhD thesis, Leipzig, Germany.
[13] Yang, K. H., Chieu, T. C., and Osofsky, S., 1989, *Appl. Phys. Lett.*, **55,** 125.
[14] Kozlovsky, M. V., and Beresnev, L. A., 1992, *Phase Trans.*, **40,** 129.